Clays Clay Miner., Vol. 70, No. 2:182–195, 2022
https://doi.org/10.1007/s42860-022-00175-8

ORIGINAL PAPER

Preparation and Properties of Antibacterial Polyhexamethylene Biguanide/Palygorskite Composites as Zearalenone Adsorbents

Yu R. Kang · B. Mu · G. Zhu · Yong F. Zhu · Ai Q. Wang

Accepted: 26 January 2022

Abstract Due to the environmental problems derived from the use of common surfactants as modifiers for clay mineral adsorbents to mitigate mycotoxin contamination of animal feeds, finding non-toxic modifiers to prepare safe and efficient adsorbents is necessary. The objective of the present study was, therefore, to modify acidified palygorskite with polyhexamethylene biguanide (PHMB) to obtain antibacterial polyhexamethylene biguanide/palygorskite (PHMB/Plg) composites for the removal of zearalenone, a common mycotoxin. The PHMB/Plg composites were characterized and analyzed by X-ray diffraction, Fourier-transform infrared spectroscopy, field-emission scanning electron microscopy, and isothermal nitrogen adsorption analysis. The adsorption properties of the composites with respect to zearalenone and their antibacterial activity with respect to *Escherichia coli* and *Staphylococcus aureus* were studied. The results indicated that the hydrophobicity of palygorskite was enhanced after modification with PHMB, which could effectively improve the adsorption property of palygorskite toward the non-polar zearalenone molecules. The adsorption capacity of PHMB/Plg increased with increasing amounts of polyhexamethylene biguanide and increasing pH. The adsorption data were described well by pseudo-second order kinetics and by the Langmuir adsorption model. The maximum adsorption capacity was 2777 μg/g. When the amount of PHMB added increased to 15 wt.%, the composites obtained exhibited good antibacterial performance, and the minimum inhibitory concentrations for *Escherichia coli* and *Staphylococcus aureus* were both at 2.5 mg/mL.

Keywords Antibacterial activity · Composite adsorbents · Palygorskite · Polyhexamethylene biguanide · Zearalenone

Y. R. Kang · B. Mu (✉) · G. Zhu · Y. F. Zhu · A. Q. Wang (✉)
Key Laboratory of Clay Mineral Applied Research of Gansu Province, Center of Eco-materials and Green Chemistry, Lanzhou Institute of Chemical Physics, Chinese Academy of Sciences, Lanzhou 730000, P. R. China
e-mail: mubin@licp.cas.cne-mail: aqwang@licp.cas.cn

Introduction

Zearalenone (ZEN) is a mycotoxin with estrogenic effects produced by *Fusarium*, which is ubiquitous in corn, wheat, sorghum, and other grains and their by-products (Fu et al. 2020; Xu et al. 2021). ZEN has strong reproductive toxicity, immune toxicity, genetic toxicity, estrogenic effects, carcinogenicity, and teratogenicity, which seriously endanger animal and human health (Gruber-Dorninger et al. 2021; Wang et al. 2019; Wu et al. 2021a). Finding a safe and effective method to remove ZEN from animal feeds, therefore, is crucial (Chang et al. 2020; Fu et al. 2020). Various methods have been developed for the removal of ZEN, including adsorption, solvent extraction, ozonation, enzymatic degradation, microorganism degradation, etc. (Wu et al. 2021b). Among them, the adsorption method is considered to be the most feasible and economical due

to the advantages of low cost and high efficiency (Li et al. 2018; Sprynskyy et al. 2012; Sun et al. 2014; Sun et al. 2018, Sun et al. 2020, Zhang et al. 2020a). Bai et al. (2017) prepared a functionalized graphene oxide composite modified with amphiphilic molecules, didodecyldimethylammonium bromide, for removal of ZEN from corn oil. Kalagatur et al. (2017) developed a type of activated carbon derived from seed shells of Jatropha curcas for adsorption of ZEN, and it exhibited an excellent binding to ZEN with a maximum adsorption capacity of 23.14 μg/mg in vitro. Surface-imprinted polymers supported by hydroxylapatite were synthesized by a molecular imprinting technique for adsorption of ZEN, and the composites displayed high sensitivity to ZEN with a maximum adsorption capacity of 6.77 μg mg^{-1} at an initial concentration of 20 μg mL^{-1} (Zhang et al. 2020b). However, the cost of these synthetic adsorbents was high, which seriously impeded their wide application in practice.

Compared with these synthesized adsorbents, natural clay minerals including montmorillonite, kaolinite, halloysite, rectorite, and other non-metallic minerals were also used as low-cost adsorbents for removal of mycotoxins because of their rich reserves and low price (Gan et al. 2019; Sadia et al. 2016; Spasojevic et al. 2021). Due to the good hydrophilic performance of these natural clays and clay minerals, achieving efficient removal of nonpolar and hydrophobic ZEN molecules is difficult. Therefore, long-chain quaternary ammonium surfactants, such as cetyltrimethyl ammonium bromide (Feng et al. 2008), dodecyltrimethylammonium bromide and cetylpyridinium chloride (Markovic et al. 2017; Sun et al. 2018; Zhang et al. 2019), octadecyldimethylbenzyl ammonium (Spasojevic et al. 2021), and stearyldimethylbenzylammonium chloride (Zhang et al. 2015) were employed to modify natural clays and clay minerals to improve the surface/interfacial compatibility between adsorbents and ZEN, which could obviously enhance the adsorption performance of clays and clay minerals with respect to ZEN. However, these long-chain surfactants presented large surface activity, medium/high toxicity, and poor biodegradability, which significantly affected the migration and bioavailability of the other coexisting pollutants even at relatively low concentration (Sandbacka et al. 2000; Teresa Garcia et al. 2016). Therefore, increasing attention has been paid to the environmental problems caused by these surfactants in many countries, and finding eco-friendly and non-toxic modifiers for the preparation of safe and efficient adsorbents for mycotoxin ZEN based on clays and clay minerals is essential.

Polyhexamethylene bisguanide (PHMB) is a new type of eco-friendly multi-functional cationic polymer (Sowlati-Hashjin et al. 2020) with the advantages of good stability, safety, and non-toxicity compared to traditional surfactants. At the same time, PHMB exhibits broad-spectrum antibacterial properties, which could effectively inhibit the growth of gram-positive bacteria, gram-negative bacteria, fungi, and yeasts (Asadi et al. 2021; Peng et al. 2021). The guanidine group was easily protonated to be positively charged, so PHMB could be adsorbed on the negatively charged bacterial cell membranes, and then destroy the cell membranes and ultimately kill bacteria (Leitgeb et al. 2013; Shi et al. 2015). Palygorskite (Plg) is a 2:1 type chain-layered hydrated magnesium-rich aluminosilicate clay mineral with nanorod-like morphology and regular nanochannel structure, and thus Plg has been widely employed as an adsorbent for adsorption and removal of cationic molecules and ions (Tian et al. 2016; Yang et al. 2018; Youcef et al. 2019). The objective of this study was, therefore, to develop novel dual-functional Plg-based adsorbents of polyhexamethylene biguanide/palygorskite (PHMB/Plg) composites possessing significant adsorption capacity for and antibacterial activity toward ZEN. The structures and surface properties of the composites were characterized using X-ray diffraction (XRD), Fourier-transform infrared spectroscopy (FTIR), field emission scanning electron microscopy (FE-SEM), zeta potential, and contact angle (*CA*) measurements. Batch adsorption experiments were conducted systematically to evaluate the adsorption properties of composites toward ZEN over various contact times, pH values, and initial concentrations. The antibacterial performances of the composites relative to *Staphylococcus aureus* (*S. aureus*) and *Escherichia coli* (*E. coli*) were also studied.

Materials and Methods

Chemicals and Materials

Plg was obtained from Huangnishan (Xuyi County, China) and acidified with 2 wt.% sulfuric acid (Xilong Chemical Factory Co., Ltd., Guangzhou, China.) at room temperature before use. The acidified Plg was composed of 2.04% CaO, 11.95% Al_2O_3, 6.67% MgO, 56.68% SiO_2, 1.77% K_2O, and 8.77% Fe_2O_3 as determined by X-ray fluorescence (XRF, PANalytical,

https://doi.org/10.1007/s42860-022-00175-8 Published online by Cambridge University Press

Almelo, The Netherlands). Polyhexamethylene biguanidine hydrochloride (PHMB) with a concentration of 20 wt.% aqueous solution was purchased from Shanghai Yuanye Biotechnology Co., Ltd. (Shanghai, China). ZEN (98%) was supplied by J&K Scientific Ltd. (Beijing, China). Acetonitrile was purchased from Lian Longbohua Pharmaceutical and Chemical Co., Ltd. (Tianjin, China). *S. aureus* (ATCC25912) and *E. coli* (ATCC25922) were provided by Lanzhou University Second Hospital (Lanzhou, China) as representative gram-negative and gram-positive bacteria. Luria-Bertani (LB) broth and Nutrient Agar (NA) medium were obtained from Qingdao Hope Bi-Technology Co., Ltd. (Qingdao, China). The solutions used in the experiment were prepared with ultrapure water.

Preparation of PHMB/Plg Composites

Plg (10.00 g) was weighed in a beaker and stirred with 50 mL of distilled water, and then 1.25, 2.50, 3.75, 5.00, or 7.50 g of PHMB aqueous solution was added, giving a PHMB content of 2.5, 5.0, 7.5, 10.0, or 15.0% of the mass of Plg, respectively. The mixtures of PHMB and Plg were heated to 60°C for 4 h, and then the solid products were centrifuged, washed with water, dried at 85°C, and finally ground and passed through a 200-mesh sieve to obtain the PHMB/Plg composites. The samples obtained were recorded as PHMB/Plg-1, PHMB/Plg-2, PHMB/Plg-3, PHMB/Plg-4, and PHMB/Plg-5 based on the amounts of PHMB added.

Characterization

FTIR spectra of the samples were recorded on a Thermo Nicolet NEXUS TM 6700 spectrophotometer (Waltham, Massachusetts, USA) in the wavenumber range 400–4000 cm^{-1} using KBr pellets. FE-SEM (JSM-6701F, JEOL, Japan) was used to study the morphology of the pure Plg and modified Plg, in which the samples were coated with a layer of gold before testing. XRD patterns were collected using an X'pert PRO X-ray power diffractometer equipped with a CuKα radiation source (40 kV, 30 mA) (PANalytical Co., Almelo, The Netherlands) at a scanning rate of 2.00°2θ/min and a step interval of about 0.167°2θ between 3 and 80°2θ. Zeta potentials of Plg samples were measured by phase analysis light scattering (Malvern Zetasizer Nano ZS, Malvern Panalytical Ltd, Malvern, UK), using disposable cuvettes. Nitrogen adsorption-desorption isotherms were studied by a Micromeritics ASAP 2020 (Norcross, Georgia, USA) specific surface area and porosity analyzer at −196°C. Before the samples were measured, they were dried at 90°C for 10 h under N_2 protection to remove the water contained in the samples. Thermogravimetric analysis (TGA) was performed on a STA8000 simultaneous thermal analyzer (PerkinElmer, Waltham, Massachusetts, USA) at a heating rate of 10°C/min under a N_2 atmosphere, the initial mass of all samples was 0.005 g. The elemental contents of C and N were determined using an organic elemental analyzer of vario EL CUBE (Elementar Analysensysteme GmbH, Langenselbold, Germany) with a gas pressure of 1100 mbar and gas flow rate of 15 mL/min.

Evaluation of Adsorption Performance

Five mg of ZEN was dissolved in 50 mL of methanol solution to prepare 100 mg/L ZEN solution. Adsorption experiments were all batch experiments. Firstly, 50 μL of ZEN solution was diluted to 10 mL, then 0.02 g of the composite was added and shaken at 37°C for 60 min in a thermostatic oscillator (THZ-98A, Shanghai Yiheng Technology Co., Ltd, Shanghai, China) with a rotating speed of 120 rpm. The solid was centrifuged for 10 min at 1001×*g* to obtain a clear liquid. Finally, the supernatant was diluted with an equal volume of methanol and filtered through a 0.22 μm membrane for high performance liquid chromatography (HPLC) analysis. The adsorbed amounts (q_e) and removal ratio (R) of ZEN were calculated according to the following formulae:

$$q_e = [V(C_0 - C_e)]/m \quad (1)$$

$$R = (1 - C_e)/C_0 \times 100\% \quad (2)$$

where q_e is the amount of ZEN adsorbed by the sample at time t or equilibrium state (μg/mg), C_0 is the initial concentration of ZEN in the solution (μg/mL), C_e is the concentration of ZEN in the solution after adsorption (μg/mL), m is the quality of the adsorbent used (g), and V is the volume of ZEN solution (mL). HPLC analysis was performed on an Agilent 1260 Infinity II, which was equipped with a quaternary pump and G7219 autosampler and C18 column (250 mm×4.6 mm×5 μm, Agilent, Santa Clara, California, USA). The mobile phase acetonitrile and water (v/v = 60/40) was pumped at a flow rate 0.6 mL/min

https://doi.org/10.1007/s42860-022-00175-8 Published online by Cambridge University Press

and a G7114A VWD detector was used for the ZEN detection (UV wavelength = 238 nm).

The effect of the added amounts of PHMB (2.5, 5, 7.5, 10, and 15%), dosage of adsorbents (5, 10, 15, 20, 30, and 40 mg), pH (2, 3, 4, 5, 6, 7, and 8), contact time (5, 10, 15, 30, 60, and 90 min), and initial concentration of ZEN (0.3, 0.5, 1.0, 2.0, 5.0, 10.0, and 20.0 μg/mL) on the adsorption of ZEN were studied systematically. The pH of ZEN solutions was adjusted with 0.5 mol/L HCl and NaOH solutions. The concentrations of ZEN before and after adsorption of ZEN were measured by HPLC according to the procedures above, while all adsorption experiments were repeated three times.

Antibacterial Performance Evaluation

The antibacterial activities of various PHMB/Plg samples against *E. coli* and *S. aureus* were evaluated by determining the minimum inhibitory concentration (MIC) according to the two-fold dilution method (Zhong et al. 2020). Typically, all the samples were weighed and placed in Petri dishes under a UV lamp for 30 min to sterilize them. NA solutions (20 mL) were sterilized at high pressure of 103.4 kPa and cooled to 60°C, and then poured into the Petri dishes with sterilized samples. After that, 1 μL of the bacterium solution with a concentration of 10^4 CFU/mL was inoculated in the Petri dishes in spots, the ultimate concentrations of PHMB/Plg samples were 5, 2.5, 1.25, and 0.625 mg/mL, respectively. Each Petri dish was inoculated with 3 spots. All Petri dishes with samples were placed in a carbon dioxide incubator for 20 h at 35°C. The minimum concentration needed to inhibit colony growth completely was the MIC value of the sample.

Evaluation of Moisture Adsorption Performance

The moisture adsorption ratio (*MAR*) of composite adsorbents was determined by gravimetric analysis. The adsorbent samples with various PHMB loadings were dried in an oven at 80°C for 6 h, and the initial mass m_0 was recorded. Next, the samples were stored in a dryer with a saturated NaCl salt solution (75% humidity) at the bottom for 72 h. The sample mass m_1 was recorded. Five specimens at least were repeated to determine the average values in order to obtain reproducible results. The *MAR* value of the sample was calculated by the following equation:

$$MAR = \frac{(m_1\text{-}m_0)}{m_0} \times 100\% \quad (3)$$

Water Contact Angles of Adsorbent

The surface modification effect of PHMB for Plg with various contents was evaluated using the water contact angles (*CA*) via a KRŰSS contact angle meter (DSA100S, Hamburg, Germany) at ambient temperature. The powder samples were pressed into tablets (Press manufactured by ZHY-40, Beijing Zhonghe Venture Technology Development Co., Ltd, Beijing, China) under a pressure of 35 MPa, and then 5 μL of water was dropped onto the tablet surface.

Results and Discussion

FESEM Analysis

The microstructures of the samples were examined by FE-SEM (Fig. 1) and revealed obvious agglomerations in the raw Plg. After modification with PHMB, the disaggregation of crystal bundles or aggregates of Plg was improved and the dispersion of Plg crystal bundles increased with increase in the PHMB content. This phenomenon was attributed to the adsorption of PHMB from the surfaces of the rod-shaped crystals, which effectively weakened the interactions (electrostatic, hydrogen-bonding, and Van der Waals forces) among the Plg crystals due to spatial steric hindrance and electrostatic interaction (Desai et al. 2010). This result was also consistent with Plg modified by acrylamide (Zuo et al. 2019).

FTIR Analysis

C=N stretching vibrations of guanidine groups were observed at 1644 cm^{-1}, and the C–N stretching vibrations appeared at 1461 and 1358 cm^{-1}, while the stretching vibration peaks of N–H were located at 3278 and 3180 cm^{-1} (Fig. 2a). The absorption bands at 2934 and 2850 cm^{-1} were attributed to the symmetric and asymmetric stretching vibration peaks of the C–H bond (–CH_2 and –CH_3). The main characteristic absorption bands of Plg did not change significantly before and after modification with PHMB, such as stretching vibrations of

https://doi.org/10.1007/s42860-022-00175-8 Published online by Cambridge University Press

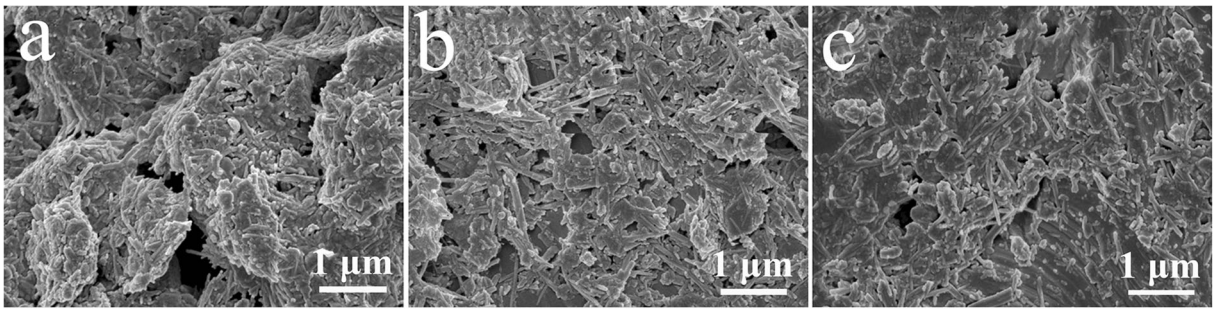

Fig. 1 SEM images of **a** Plg, **b** PHMB/Plg-2, and **c** PHMB/Plg-4 composites

Al(Mg)–O–H at 3614 cm^{-1}, of octahedral edge crystal water at 3551 cm^{-1}, the antisymmetric stretching vibrations of Si–O–Si at 1196 and 1030 cm^{-1}, the symmetric stretching vibration peak of Si–O–Si at 783 cm^{-1}, the superposition of peaks from Si–O–Mg and Si–O–Al groups at 685 cm^{-1}, the bending vibration of Si–O–Si at 514 cm^{-1}, and the bending vibration peak of O–Si–O at 469 cm^{-1} (Mu et al. 2013; de Brito Buriti et al. 2022). However, several new bands from the PHMB/Plg composites appeared, including the C–H bond ($-CH_2$, $-CH_3$) and C–N bond at 2941 and 2865 cm^{-1}, 1472 and 1361 cm^{-1}, respectively (Wang et al. 2015; Wang et al. 2018). In addition, the absorption peak of the N–H group in PHMB overlapped with the stretching vibration of zeolite water and surface adsorbed water at 3405 cm^{-1} in Plg, while the stretching vibration of C=N in PHMB overlapped with the bending vibration peak of zeolitic water and surface adsorbed water at 1646 cm^{-1}. With the increase in the PHMB content, the relative intensities of these peaks increased gradually. These results suggested that PHMB was anchored successfully on the surface of Plg through hydrogen bond and electrostatic interaction (Buriti et al. 2021; Zhuang et al. 2017).

XRD Analysis

The XRD patterns revealed peaks at 8.50, 19.90, 27.58, and 34.52°2θ (Fig. 2b) corresponding to the (110), (040), (400), and (102) crystal planes of Plg. The diffraction peaks at 20.83 and 26.59°2θ were characteristic of quartz (Dong et al. 2019). The diffraction peaks of the PHMB/Plg composites were almost the same as for the raw Plg, suggesting that the crystal structure of Plg was largely unchanged by the PHMB modification.

Pore Structural Parameters

Measurements of the specific surface area and pore-structure parameters of Plg and PHMB/Plg composites (Table 1) found an overall decreasing trend in S_{BET} after treatment with various concentrations of PHMB, especially S_{micro} and V_{micro}. When the ammount of PHMB added was >7.5%, the micropore specific surface area derived from a *t*-plot disappeared, and it might be ascribed to the coverage of the long alkyl chain, which reduced the adsorption of N_2. The pore size increased with added amounts of PHMB, however, which might be due to the long distance between each PHMB molecule on the surface of Plg (Dong et al. 2011).

Zeta Potential Analysis

The zeta potentials (Fig. 2c) of the PHMB/Plg changed from negative to positive values with increasing PHMB dosage. Plg is well known to be negatively charged and thus the cationic PHMB molecules with guanidine groups are adsorbed easily through hydrogen bonding and electrostatic forces, thus reducing the negative charge and even changing the zeta potential from negative to positive as the PHMB loading increased. When the PHMB loading exceeded 10%, the zeta potential remained unchanged, indicating that the PHMB loading on Plg reaches a saturation point or maximum level.

Thermogravimetry (TG) and Elemental Analysis

Thermal gravimetric analysis (Fig. 2d) revealed an initial weight loss in Plg between 30 and 200°C due to removal of physically adsorbed water and zeolitic water confined within the nanochannels of Plg. A similar phenomenon was also observed in the PHMB/Plg composites, but the weight loss in this region was much

https://doi.org/10.1007/s42860-022-00175-8 Published online by Cambridge University Press

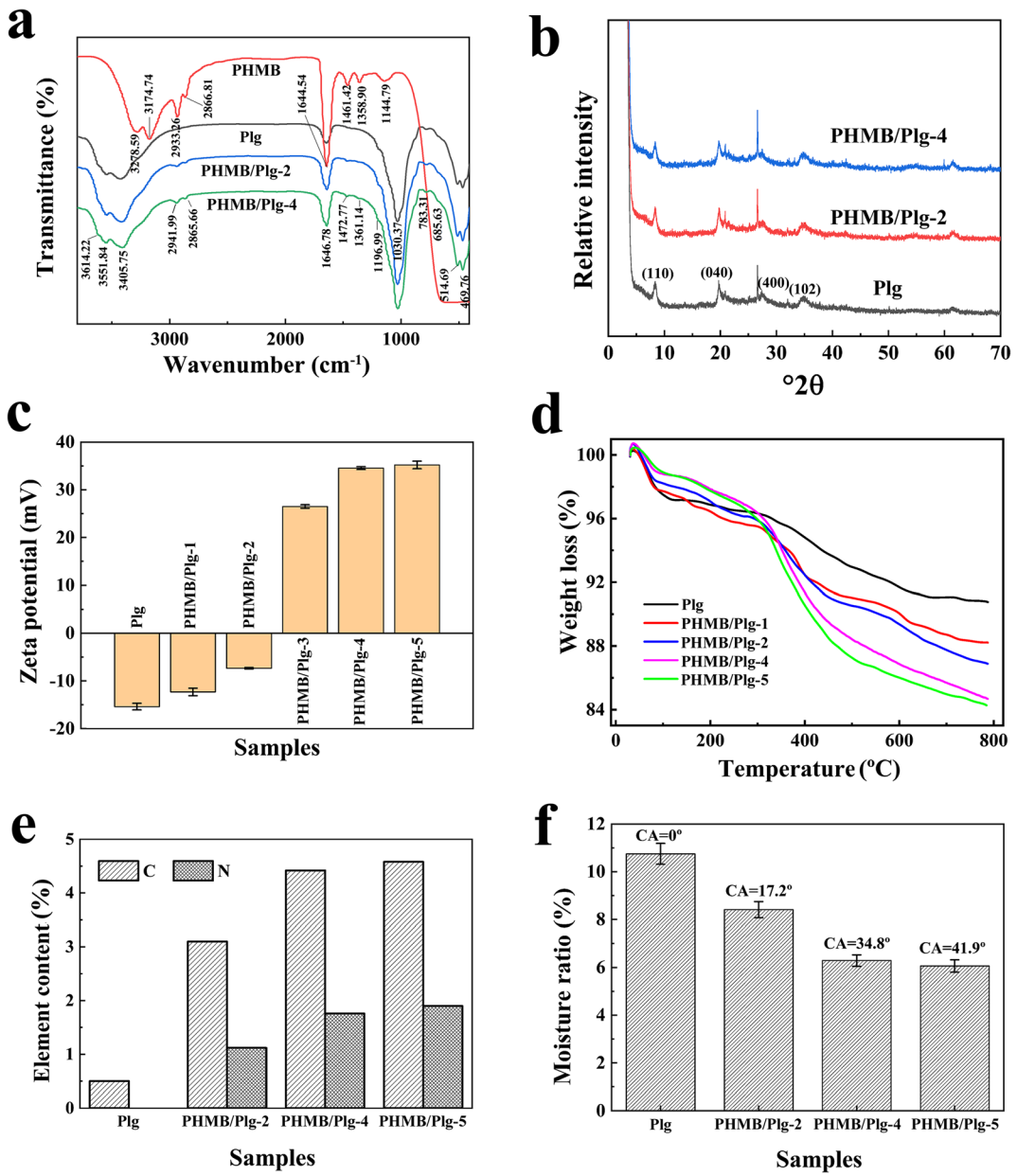

Fig. 2 **a** FTIR spectra of PHMB, Plg, and PHMB/Plg composites. **b** XRD patterns of Plg and PHMB/Plg composites. **c** Zeta potential of Plg and PHMB/Plg composites. **d** TGA curves of Plg and PHMB/Plg composites. **e** C and N contents of PHMB/Plg composites with amounts of PHMB added. **f** Moisture adsorption ratio and *CA*s of Plg and PHMB/Plg composites

smaller than in the raw Plg (Table 2), suggesting that the Plg surface was covered with PHMB and that the surface changed from hydrophilic to hydrophobic after modification. The weight loss between 200 and 500°C was attributed mainly to the removal of the bound water and coordinated water, and the thermal decomposition of the loaded PHMB. Compared with Plg, the increased weight losses of the PHMB/Plg composites in this region was further evidence for increased PHMB loading. The weight loss from 500 to 800°C was due to the dehydroxylation of structural OH in the Plg and the further decomposition of residual organic matter in PHMB/Plg composites. As expected, the weight loss from the PHMB/Plg composites increased with increasing loading of PHMB.

https://doi.org/10.1007/s42860-022-00175-8 Published online by Cambridge University Press

Table 1 Pore-structure parameters of Plg and PHMB/Plg composites

Samples	S_{BET}[a] (m^2/g)	S_{micro}[b] (m^2/g)	S_{ext}[c] (m^2/g)	V_{micro}[d] (cm^3/g)	V_{total}[e] (cm^3/g)	PZ[f] (nm)
Plg	219.87	68.79	151.09	0.0308	0.3276	5.96
PHMB/Plg-1	209.63	48.44	161.19	0.02057	0.3060	5.84
PHMB/Plg-2	174.45	25.04	149.41	0.0094	0.2750	6.31
PHMB/Plg-3	117.14	-	117.97	-0.0026	0.2174	7.42
PHMB/Plg-4	95.76	-	104.41	-0.0061	0.2092	8.74
PHMB/Plg-5	108.29	-	133.05	-0.0147	0.2497	9.22

[a] BET (Brunauer-Emmett-Teller) surface area

[b] Mesopore surface area, calculated using BJH method from desorption curve

[c] Micropore surface area, derived from t-plot method

[d] Micropore volume

[e] Total pore volume, measured at $P/P_0 = 0.995$

[f] Average pore diameter, calculated according to BET

The increased loading of PHMB was further confirmed by the elemental analysis (Fig. 2e), revealing increases in the C and N contents from 3.1to 4.58% and 1.12 to 1.90%, respectively, as the amount of PHMB increased from 5 to 15%. When the PHMB content was >10 wt.%, the C and N contents increased very slowly, indicating that the loading of PHMB on Plg gradually reached a saturation point.

Surface Hydrophobicity Analysis

Many studies have confirmed that organically modified clays or clay minerals could improve the adsorption capacity for ZEN because the organic modification increased the surface hydrophobicity (Spasojevic et al. 2021; Sun et al. 2020). The change in *MAR* values of PHMB/Plg (Fig. 2f) with increasing PHMB resulted in less moisture adsorption, indicating that the hydrophobicity of Plg was enhanced. The less polar surface was beneficial for capturing non-polar ZEN molecules through hydrophobic interactions, thereby enhancing the adsorption capacity toward ZEN (Zhang et al. 2019). The hydrophobicity of the modified samples was also confirmed by contact-angle measurements. Water droplets were adsorbed immediately after being dripped on pure Plg due to the high hydrophilicity. The *CA* values of PHMB/Plg composites increased with increasing PHMB content, which indicated that the wettability of Plg with water decreased and the surface hydrophobicity increased after PHMB modification. However, the *CA* values of PHMB/Plg composites were still lower than 50°. This phenomenon was ascribed to the strong hydrophilicity of PHMB; part of hydrophilic groups with positive charge took part in the interaction with the Si–OH of Plg in the modification process, but the remainder was still exposed to the outside.

Table 2 Weight loss of Plg and the PHMB/Plg composites over various temperature ranges

Samples	Weight Loss (wt.%) over Temperature Range			
	30–200°C	200–500°C	500–800°C	∑(30–800°C)
Plg	3.13	3.92	2.19	9.24
PHMB/Plg-1	3.48	5.53	2.77	11.78
PHMB/Plg-2	2.90	6.59	3.62	13.11
PHMB/Plg-4	2.18	9.39	3.75	15.32
PHMB/Plg-5	2.25	10.45	3.02	15.72

https://doi.org/10.1007/s42860-022-00175-8 Published online by Cambridge University Press

Adsorption Properties of PHMB/Plg Composites

Effect of PHMB Content

The amount of PHMB loaded was an important factor affecting the adsorption capacity of the composite adsorbents toward ZEN, which was directly related to the amount of PHMB added (Fig. 3a) and is probably attributable to the increase in surface hydrophobicity as the amount of PHMB increased. The sequestration of hydrophobic ZEN was enhanced due to the principle of polar similar solubility. When the amount of PHMB added surpassed 10%, however, the removal capacity scarcely changed. Sample PHMB/Plg-4 was chosen, therefore, as the sample with which to study the relevant adsorption conditions.

Effect of Adsorbent Dosage

The removal ratio (R) of PHMB/Plg composites toward ZEN increased gradually with increase in the dosage of composite used (Fig. 3b). This was due to the increase in the number of active adsorption sites for ZEN with the amount of composite added. When the dosage of the composite increased from 5 to 40 mg, the value of R increased from 63.36 to 95.28%; when the dosage exceeded 20 mg, the removal ratio increased slightly. It indicated that the adsorbed amount of ZEN on the surface of the composite reached a dynamic equilibrium with the concentration of ZEN in the solution, adsorption equilibrium was achieved, and thus the optimal dosage of composite was 20 mg.

Effect of pH

In order to simulate the acid-base environment of an animal's gastrointestinal tract, a pH of ~2–8 was selected for the adsorption experiment. As illustrated in Fig. 3c, the removal ratio of composite adsorbents to ZEN increased rapidly when the pH increased from 2 to 4, and then the removal ratio of ZEN hardly changed as the pH exceeded 5, indicating that the hydrophobic effect of PHMB modification might be more important than the charge change (Fig. 2c). This behavior was also consistent with the results of a previous study (Feng et al. 2008); the hydrophobic property of composite adsorbents was mainly responsible for the specific adsorption of ZEN..

Effect of Contact Time and Adsorption Kinetics

The effect of contact time on the adsorption capacity of the composites for ZEN (Fig. 3d) revealed that when the contact time was <5 min the removal ratio reached 85.94%, then it increased to 89.37% as the contact time increased to 45 min, and finally almost no obvious change occurred by 90 min. From these observations, one may infer that a large adsorption affinity existed between the composite and the ZEN, and thus the composite could quickly interact with ZEN molecules in a short time to achieve the adsorption equilibrium (Hachemaoui et al. 2020).

In addition, the experimental data were fitted using pseudo-first order (Eq. 4) and pseudo-second order (Eq. 5) kinetics, to see if these could provide a mechanism for the adsorption of ZEN on PHMB/Plg composites.

$$\log q_e - q_t = q_e - \frac{k_1}{2.303} t \tag{4}$$

$$\frac{t}{q_t} = \frac{1}{k_2 q_e^2} + \frac{t}{q_e} \tag{5}$$

where q_e (μg/g) and q_t (μg/g) denote the amounts of ZEN adsorbed on the PHMB/Plg composites at equilibrium and time t (min), respectively; k_1 (min^{-1}) and k_2 ((g/μg)/min) are the rate constants for the pseudo-first order and pseudo-second order adsorption equations, respectively. The correlation coefficients (R) and the rate constants (k_1 and k_2) obtained from the plot of experiment data are listed in Table 3.

The R_2^2 value of the pseudo-second order kinetics model was 0.9999, and the calculated values for q_e (denoted $q_{e,cal}$) were closer to the experimental values (denoted $q_{e,exp}$) than they were in the pseudo-first order kinetics model, indicating that the pseudo-second order model could well describe the removal of ZEN by PHMB/Plg composites, and thus the major adsorption mechanism would appear to be chemisorption (Zhang et al. 2019).

Effect of Initial Concentration and Adsorption Isotherms

Generally, the adsorption performance of the adsorbent depends on the initial concentration of the adsorbed substance solution. Figure 3e exhibits the effect of different initial concentrations on the adsorption capacity

https://doi.org/10.1007/s42860-022-00175-8 Published online by Cambridge University Press

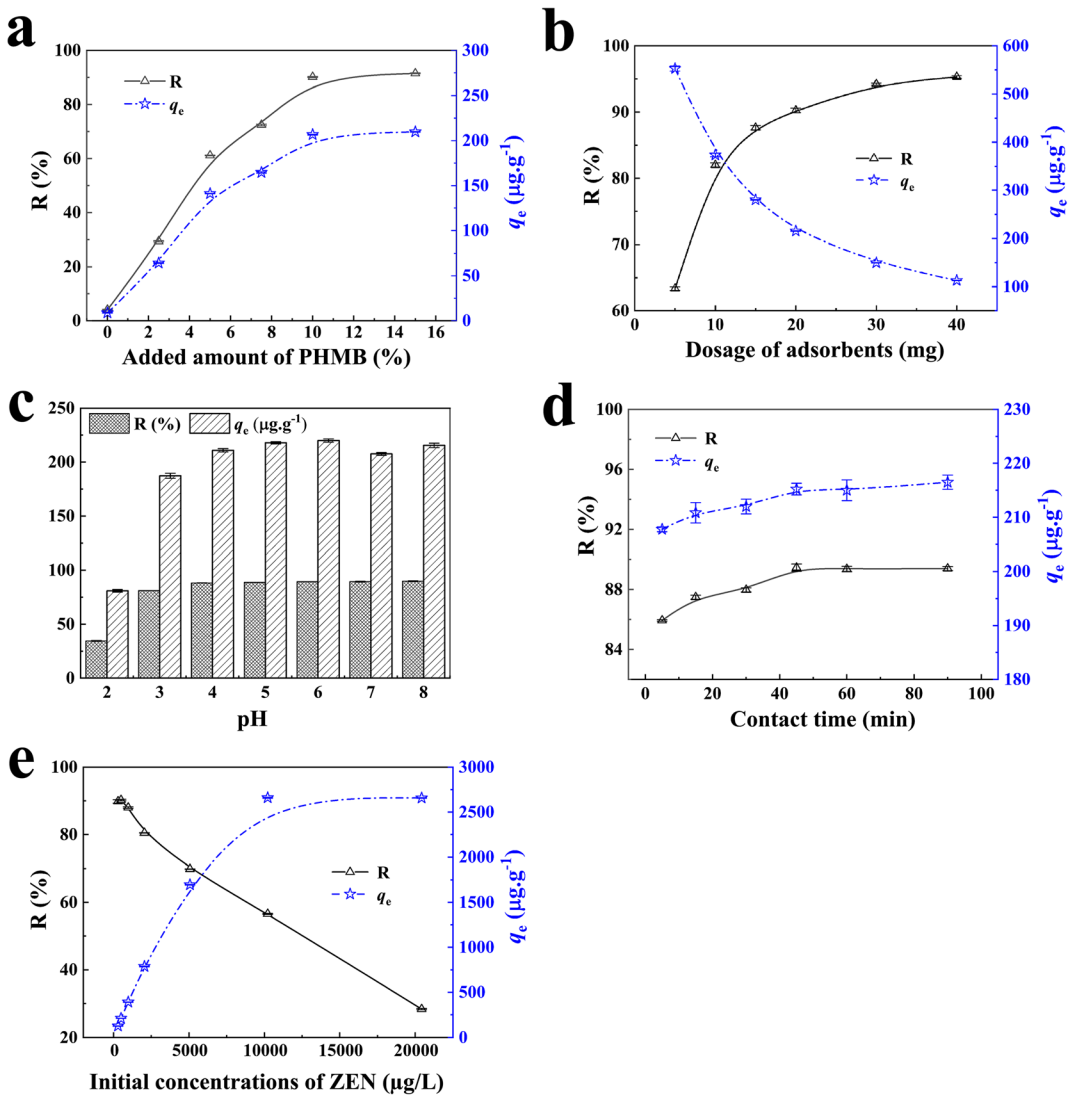

Fig. 3 **a** Effect of PHMB content on the amount of ZEN adsorbed (C_0 = 467.82 μg/L, V = 10 mL, m = 20 mg, t = 60 min, T = 37°C, pH = 6). **b** Effect of adsorbent dosage on the adsorption of ZEN (C_0 = 482.52 μg/L, V = 10 mL, t = 60 min, T = 37°C, pH = 6). **c** Effect of pH on the adsorption of ZEN (C_0 = 497.48 μg/L, m = 20 mg, V = 10 mL, T = 37°C, t = 60 min). **d** Effect of contact time on the adsorption of ZEN on PHMB/Plg-4 (C_0 = 489.20 μg/L, m = 20 mg, V = 10 mL, T = 37°C, pH = 6). **e** Effect of various initial concentrations of ZEN on the adsorption of ZEN on PHMB/Plg-4 (m = 20 mg, V = 10 mL, T = 37°C, t = 60 min, pH = 6)

Table 3 Parameters from adsorption kinetics, Langmuir and Freundlich constants, and correlation coefficients associated with adsorption isotherms of Plg and PHMB/Plg composites

$q_{e,exp}$ (μg/g)	Pseudo- first -order model			Pseudo- second -order model		
	$q_{e,cal}$ (μg/g)	k_1 (min^{-1})	R_1^2	$q_{e,cal}$ (μg/g)	k_2 (g/μg)/min	R_2^2
217.95	17.13	0.0444	0.8924	215.51	0.0103	0.9999
$q_{e,exp}$ (μg/g)	Langmuir model			Freundlich model		
	$q_{e,cal}$ (μg/g)	K_L (L/μg)	R_L^2	K_F	n	R_F^2
2659.94	2777.77	0.0014	0.9975	0.0309	1.9646	0.9520

https://doi.org/10.1007/s42860-022-00175-8 Published online by Cambridge University Press

of PHMB/Plg composites for ZEN. The initial concentration of ZEN solution played an important role in the adsorption process. With the increase in solution concentration, the adsorption capacity of PHMB/Plg composites for ZEN increased gradually. This was due to the fact that a greater concentration of the solution produces a greater driving force for adsorption. Furthermore, the adsorption gradually tended to equilibrium as the adsorption sites were occupied by ZEN molecules.

Langmuir (Eq. 6) and Freundlich (Eq. 7) adsorption models were used to fit the equilibrium adsorption experimental data. The Langmuir model assumed that the adsorbent presented a homogeneous structure, where all adsorption sites are equivalent.

$$\frac{C_e}{q_e} = \frac{1}{q_{\max} b} + \frac{C_e}{q_{\max}} \quad (6)$$

where q_e represents the equilibrium adsorption capacity of ZEN on PHMG/Plg composites (μg/g), C_e denotes the equilibrium ZEN concentration (μg/L), $q_{\max}$ and b are the monolayer adsorption capacity of the adsorbent and Langmuir adsorption constant (L/μg), respectively.

The Freundlich empirical model removes the homogeneity of sites constraint, thus allowing for heterogeneous systems to be described by a factor of $1/n$ under reversible adsorption conditions.

$$\log q_e = \frac{1}{n}\log C_e + \log \mathrm{K} \quad (7)$$

where q_e represents the amount of ZEN adsorbed at equilibrium (μg/g), C_e is the final ZEN concentration at equilibrium (μg/L), K is the Freundlich isotherm constant (L/μg), and $1/n$ is the heterogeneity factor. The Langmuir and Freundlich parameters obtained from the plot of the experimental data are listed in Table 3. The correlation coefficient R^2 obtained from the Langmuir model was greater than that of Freundlich, and the theoretical maximum adsorption capacity closely followed the actual experimental value. These observations indicate that the removal of ZEN by PHMB/Plg composites was more in line with the Langmuir than the Freundlich model, and thus a monoloayer of ZEN may have formed on the PHMB/Plg composites, and the maximum adsorption capacity was 2777 μg/g. This conclusion was consistent with the conclusions of Sun et al. (2018) and Li et al. (2014).

The adsorption performance of the adsorbents in the present study was compared with the relevant clay mineral-based adsorbents described in the literature (Table S1). PHMB/Plg composites exhibited a much better performance than polyvinylpyrrolidone, cholestyramine, and raw silicate minerals, but the adsorption capacity was less than that of silicate minerals modified by traditional surfactants. This may be due to the relatively small cation exchange capacity (CEC) of Plg (10.49 meq/100 g) compared with rectorite and montmorillonite at 46.36 and ~68.29–104 meq/100 g, respectively. The smaller adsorption capacity may also be due,

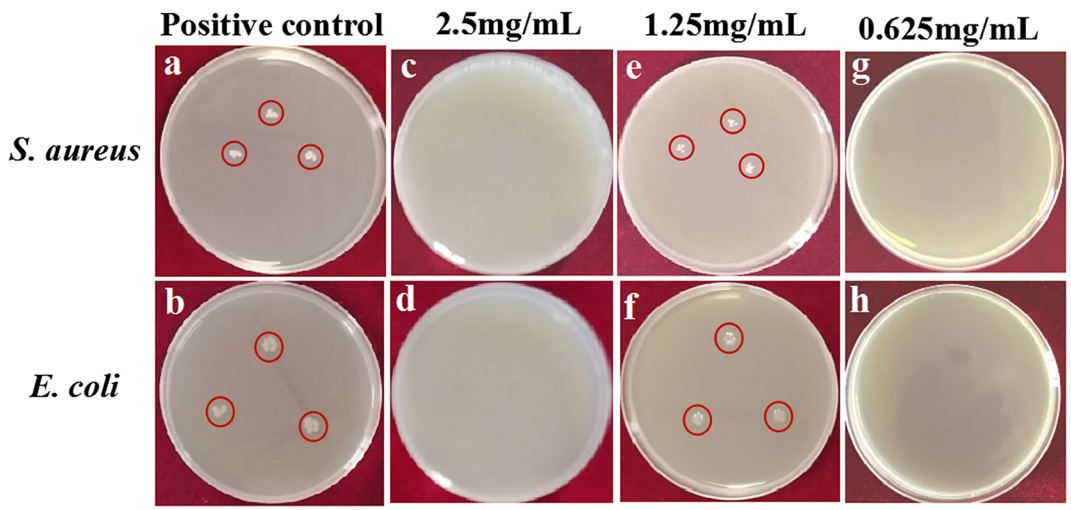

Fig. 4 a and **b** Positive control of *S. aureus* and *E. coli*; **c** and **e***S. aureus* treated with PHMB/Plg-5 at the concentrations of 2.5 mg/mL and 1.25 mg/mL, respectively; **d** and **f***E. coli* treated with PHMB/Plg-5 at the concentrations of 2.5 mg/mL and 1.25 mg/mL, respectively; **g** and **h***S. aureus* and *E. coli* treated with PHMB at the concentrations of 0.625 mg/mL, respectively.

https://doi.org/10.1007/s42860-022-00175-8 Published online by Cambridge University Press

in part, to the small amount of organic matter naturally present in Plg.

Antibacterial Performance of PHMB/Plg Composites

PHMB was a kind of cationic antibacterial polymer containing guanidine groups in the main chain. It could be adsorbed on the negatively charged microbial cell membrane, leading to the leakage of K^+ and other components within the cytoplasmic fluid, and then destroyed the cell membrane (Dilamian et al. 2013). In order to evaluate the antibacterial properties of PHMB/Plg composites, *E. coli* and *S. aureus* were selected as model strains for detection. The MIC values of Plg, PHMB, and PHMB/Plg composites are listed in Table S2 and Fig. 4. Plg had no obvious antibacterial activity against *E. coli* or *S. aureus* in a previous study (Hui et al. 2019), and the MIC values of Plg against *E. coli* and *S. aureus* were >50 mg/mL. On the contrary, PHMB displayed excellent antibacterial properties, and the MIC values of PHMB against *E. coli* and *S. aureus* were <0.625 mg/mL. The surfaces of both *E. coli* and *S. aureus* were negatively charged, which could be adsorbed onto the antibacterial materials with positively charged surfaces through electrostatic interaction (Hui et al. 2020). The antibacterial activity of the PHMB/Plg composites clearly depended heavily on the loading amount of PHMB on Plg. When the amount of PHMB added was >15%, the composite exhibited good antibacterial properties, and the MIC values of *E. coli* and *S. aureus* were both at 2.5 mg/mL. The possible antibacterial mechanism of the composites was ascribed mainly to the contact between bacteria and modified Plg (Hui et al. 2020). When the amount of PHMB added was small, the guanidine group on the PHMB bonded with hydroxyl groups on the surface of Plg through hydrogen bonding and electrostatic action. As the amount of PHMB added increased gradually, some of the guanidine groups on the PHMB could be free, allowing the PHMB/Plg composites with high PHMB loading to display a high positive charge. The bacteria could then be adsorbed on the surface of PHMB/Plg composites via electrostatic interaction, thus restricting the bacterial motion. The PHMB/Plg adsorbents, therefore, may be promising candidates as feed additives for animal breeding due to the good adsorption properties for ZEN and antibacterial activity against *E. coli* and *S. aureus*.

Conclusions

Novel ZEN adsorbents of PHMB/Plg composites with antibacterial properties were prepared successfully with PHMB as the non-toxic organic modifier. After PHMB modification, the dispersion of Plg crystal bundles and the hydrophobicity of Plg were improved. These improvements enhanced the adsorption capacity of PHMB/Plg composites for ZEN. With the increase in loading content of PHMB and pH, the adsorption capacity of composites for ZEN increased, and the adsorption could reach equilibrium within 45 min. The adsorption process was modeled best by pseudo-second order kinetics and by the Langmuir adsorption model. The maximum adsorption capacity was ~2777 μg/g. Furthermore, the PHMB/Plg composites exhibited a certain antibacterial effect when the amount of PHMB added increased to 15%, and the MIC value against *S. aureus* and *E. coli* was 2.5 mg/mL.

Acknowledgments This work was supported by the Regional Key Project of the Science and Technology Service of the Chinese Academy of Sciences (KFJ-STS-QYZX-086) and the Major Projects of the Natural Science Foundation of Gansu, China (18JR4RA001).

Funding Funding sources are as stated in the Acknowledgments.

Declarations

Conflict of Interest The authors declare that they have no conflict of interest.

References

Asadi, L., Mokhtari, J., & Abbasi, M. (2021). An alginate-PHMB-AgNPs based wound dressing polyamide nanocomposite with improved antibacterial and hemostatic properties. *Journal of Materials Science: Materials in Medicine, 32*(1), 1–11. https://doi.org/10.1007/s10856-020-06484-5

Bai, X. J., Sun, C. P., Xu, J., Liu, D., Han, Y. Y., Wu, S. L., & Luo, X. H. (2017). Detoxification of zearalenone from corn oil by adsorption of functionalized GO systems. *Applied Surface Science, 430*, 198–207. https://doi.org/10.1016/j.apsusc.2017.06.055

Chang, X. J., Liu, H. J., Sun, J., Wang, J., Zhao, C. C., Zhang, W., Zhang, J., & Sun, C. P. (2020). Zearalenone removal from

corn oil by an enzymatic strategy. *Toxins, 12*(2), 117. https://doi.org/10.3390/toxins12020117

de Brito Buriti, B. M. A., Barsosa, M. E., da Silva Buriti, J., de Melo Cartaxo, J., Ferreira, H. S., & de Araújo Neves Cartaxo, G. (2022). Modification of palygorskite with cationic and nonionic surfactants for use in oil-based drilling fluids. *Journal of Thermal Analysis and Calorimetry*, 1–11. https://doi.org/10.1007/s10973-021-10701-w

Desai, H., Biswal, N. R., & Paria, S. (2010). Rheological behavior of pyrophyllite-water slurry in the presence of anionic, cationic, and nonionic surfactants. *Industrial & Engineering Chemistry Research, 49*(11), 5400–5406. https://doi.org/10.1021/ie901643s

Dilamian, M., Montazer, M., & Masoumi, J. (2013). Antimicrobial electrospun membranes of chitosan/poly(ethylene oxide) incorporating poly(hexamethylene biguanide) hydrochloride. *Carbohydrate Polymers, 94*(1), 364–371. https://doi.org/10.1016/j.carbpol.2013.01.059

Dong, R., Liu, Y. F., Wang, X. G., & Huang, J. H. (2011). Adsorption of sulfate ions from aqueous solution by surfactant-modified palygorskite. *Journal of Chemical and Engineering Data, 56*(10), 3890–3896. https://doi.org/10.1021/je200544n

Dong, W. K., Lu, Y. S., Wang, W. B., Zong, L., Zhu, Y. F., Kang, Y. R., & Wang, A. Q. (2019). A new route to fabricate high-efficient porous silicate adsorbents by simultaneous inorganic-organic functionalization of low-grade palygorskite clay for removal of Congo red. *Microporous and Mesoporous Materials, 277*, 267–276. https://doi.org/10.1016/j.micromeso.2018.11.013

Feng, J. L., Mei, S., Du, H. H., Han, X. Y., & Xu, Z. R. (2008). In vitro adsorption of zearalenone by cetyltrimethyl ammonium bromide-modified montmorillonite nanocomposites. *Microporous and Mesoporous Materials, 113*(1-3), 99–105. https://doi.org/10.1016/j.micromeso.2007.11.007

Fu, H., Liu, J. P., Xu, W., Wang, H. X., Liao, S. H., & Chen, G. T. (2020). A new type of magnetic molecular imprinted material combined with beta-cyclodextrin for the selective adsorption of zearalenone. *Journal of Materials Chemistry B, 8*(48), 10966–10976. https://doi.org/10.1039/D0TB02146F

Gan, F. Q., Hang, X. S., Huang, Q. Y., & Deng, Y. J. (2019). Assessing and modifying China bentonites for aflatoxin adsorption. *Applied Clay Science, 168*, 348–354. https://doi.org/10.1016/j.clay.2018.12.001

Gruber-Dorninger, C., Faas, J., Doupovec, B., Aleschko, M., Stoiber, C., Hobartner-Gussl, A., Schondorfer, K., Killinger, M., Zebeli, Q., & Schatzmayr, D. (2021). Metabolism of zearalenone in the rumen of dairy cows with and without application of a zearalenone-degrading enzyme. *Toxins, 13*(2), 84. https://doi.org/10.3390/toxins13020084

Hachemaoui, M., Boukoussa, B., Mokhtar, A., Me Kki, A., Beldjilali, M., Benaissa, M., Zaoui, F., Hakiki, A., Chaibi, W., Sassi, M., & Hamacha, R. B. (2020). Dyes adsorption, antifungal and antibacterial properties of metal loaded mesoporous silica: Effect of metal and calcination treatment. *Materials Chemistry and Physics, 256*, 123704. https://doi.org/10.1016/j.matchemphys.2020.123704

Hui, A. P., Dong, S. Q., Kang, Y. R., Zhou, Y. M., & Wang, A. Q. (2019). Hydrothermal fabrication of spindle-shaped ZnO/palygorskite nanocomposites using nonionic surfactant for enhancement of antibacterial activity. *Nanomaterials, 9*, 1453. https://doi.org/10.3390/nano9101453

Hui, A. P., Yan, R., Wang, W. B., Wang, Q., & Wang, A. Q. (2020). Incorporation of quaternary ammonium chitooligosaccharides on ZnO/palygorskite nanocomposites for enhancing antibacterial activities. *Carbohydrate Polymers, 247*, 116685. https://doi.org/10.1016/j.carbpol.2020.116685

Kalagatur, N. K., Karthick, K., Allen, J. A., Nirmal Ghosh, O. S., Chandranayaka, S., Gupta, V. K., & Mudili, V. (2017). Application of activated carbon derived from seed shells of Jatropha curcas for decontamination of zearalenone mycotoxin. *Frontiers in Pharmacology, 8*, 760. https://doi.org/10.3389/fphar.2017.00760

Leitgeb, J., Schuster, R., Eng, A. H., Yee, B. N., Teh, Y. P., Dosch, V., & Assadian, O. (2013). In-vitro experimental evaluation of skin-to-surface recovery of four bacterial species by antibacterial and non-antibacterial medical examination gloves. *Antimicrobial Resistance and Infection Control, 2*, 1–6. https://doi.org/10.1186/2047-2994-2-27

Li, Y., Tian, G. Y., Dong, G. Y., Bai, S. S., Han, X. Y., Liang, J. S., Meng, J. P., & Zhang, H. (2018). Research progress on the raw and modified montmorillonites as adsorbents for mycotoxins: A review. *Applied Clay Science, 163*, 299–311. https://doi.org/10.1016/j.clay.2018.07.032

Li, Y. J., Zeng, L., Zhou, Y., Wang, T. F., & Zhang, Y. J. (2014). Preparation and characterization of montmorillonite intercalation compounds with quaternary ammonium surfactant: Adsorption effect of zearalenone. *Journal of Nanomaterials, 2014*, 167402. https://doi.org/10.1155/2014/167402

Markovic, M., Dakovic, A., Rottinghaus, G. E., Petkovic, A., Kragovic, M., Krajisnik, D., & Milic, J. (2017). Ochratoxin a and zearalenone adsorption by the natural zeolite treated with benzalkonium chloride. *Colloids and Surfaces A Physicochemical and Engineering Aspects, 529*, 7–17. https://doi.org/10.1016/j.colsurfa.2017.05.054

Mu, B., Kang, Y. R., & Wang, A. Q. (2013). Preparation of a polyelectrolyte-coated magnetic attapulgite composite for the adsorption of precious metals. *Journal of Materials Chemistry A, 1*, 4804–4811. https://doi.org/10.1039/c3ta01620j

Peng, J. M., Liu, P. M., Peng, W., Sun, J., Dong, X. H., Ma, Z. Z., Gan, D. L., Liu, P. S., & Shen, J. (2021). Poly(hexamethylene biguanide) (PHMB) as high-efficiency antibacterial coating for titanium substrates. *Journal of Hazardous Materials, 411*, 125110. https://doi.org/10.1016/j.jhazmat.2021.125110

Sadia, A., Dykes, L., & Deng, Y. J. (2016). Transformation of adsorbed aflatoxin b-1 on smectite at elevated temperatures. *Clays and Clay Minerals, 64*(3), 220–229. https://doi.org/10.1346/CCMN.2016.0640306

Sandbacka, M., Christianson, I., & Isomaa, B. (2000). The acute toxicity of surfactants on fish cells, daphnia magna and fish–a comparative study. *Toxicology in Vitro An International*

Journal Published in Association with Bibra, 14(1), 61–68. https://doi.org/10.1016/S0887-2333(99)00083-1

Shi, L. X., Zhang, W., Yang, K., Shi, H. G., Li, D., Liu, J., Ji, J. H., & Chu, P. K. (2015). Antibacterial and osteoinductive capability of orthopedic materials via cation-π interaction mediated positive charge. *Journal of Materials Chemistry B, 3*(5), 733–737. https://doi.org/10.1039/C4TB01924E

Sowlati-Hashjin, S., Carbone, P., & Karttunen, M. (2020). Insights into the polyhexamethylene biguanide (phmb) mechanism of action on bacterial membrane and dna: A molecular dynamics study. *Journal of Physical Chemistry B, 124*(22), 4487–4497. https://doi.org/10.1021/acs.jpcb.0c02609

Spasojevic, M., Dakovic, A., Rottinghaus, G. E., Obradovic, M., Krajisnik, D., Markovic, M., & Krstic, J. (2021). Influence of surface coverage of kaolin with surfactant ions on adsorption of ochratoxin a and zearalenone. *Applied Clay Science, 205*, 106040. https://doi.org/10.1016/j.clay.2021.106040

Sprynskyy, M., Gadzala-Kopciuch, R., Nowak, K., & Buszewski, B. (2012). Removal of zearalenone toxin from synthetics gastric and body fluids using talc and diatomite: A batch kinetic study. *Colloids & Surfaces B Biointerfaces, 94*, 7–14. https://doi.org/10.1016/j.colsurfb.2011.12.024

Sun, X. L., He, X. X., Xue, K. S., Li, Y., Xu, D., & Qian, H. (2014). Biological detoxification of zearalenone by aspergillus Niger strain FS10. *Food and Chemical Toxicology, 72*, 76–82. https://doi.org/10.1016/j.fct.2014.06.021

Sun, Z. M., Lian, C., Li, C. Q., & Zheng, S. L. (2020). Investigations on organo-montmorillonites modified by binary nonionic/zwitterionic surfactant mixtures for simultaneous adsorption of aflatoxin B1 and zearalenone. *Journal of Colloid and Interface Science, 565*, 11–22. https://doi.org/10.1016/j.jcis.2020.01.013

Sun, Z. M., Song, A. K., Wang, B., Wang, G. F., & Zheng, S. L. (2018). Adsorption behaviors of aflatoxin B1 and zearalenone by organo-rectorite modified with quaternary ammonium salts. *Journal of Molecular Liquids, 264*, 645–651. https://doi.org/10.1016/j.molliq.2018.05.091

Teresa Garcia, M., Kaczerewska, O., Ribosa, I., Brycki, B., Materna, P., & Drgas, M. (2016). Biodegradability and aquatic toxicity of quaternary ammonium-based gemini surfactants: Effect of the spacer on their ecological properties. *Chemosphere, 154*, 155–160. https://doi.org/10.1016/j.chemosphere.2016.03.109

Tian, G. Y., Wang, W. W., Zong, L., Kang, Y. R., & Wang, A. Q. (2016). A functionalized hybrid silicate adsorbent derived from naturally abundant low-grade palygorskite clay for highly efficient removal of hazardous antibiotics. *Chemical Engineering Journal, 293*, 376–385. https://doi.org/10.1016/j.cej.2016.02.035

Wang, J. H., Liu, S. C., Tang, W., & Ma, H. R. (2015). Enhanced removal of humic acid from aqueous solution by adsorption on surfactant-modified palygorskite. *Journal of Chemical Engineering of Japan, 48*(12), 953–959. https://doi.org/10.1252/jcej.14we436

Wang, T. T., Chen, Y. H., Ma, J. F., Jin, Z. F., Chai, M. S., Xia, X. W., Zhang, L. H., & Zhang, Y. K. (2018). A polyethyleneimine-modified attapulgite as a novel solid support in matrix solid-phase dispersion for the extraction of cadmium traces in seafood products. *Talanta: The International Journal of Pure and Applied Analytical Chemistry, 180*, 254–259. https://doi.org/10.1016/j.talanta.2017.12.059

Wu, F. Y., Cui, J., Yang, X. Y., Liu, S. D., Han, S. J., & Chen, B. J. (2021a). Effects of zearalenone on genital organ development, serum immunoglobulin, antioxidant capacity, sex hormones and liver function of prepubertal gilts. *Toxicon, 189*, 39–44. https://doi.org/10.1016/j.toxicon.2020.11.005

Wu, N., Ou, W., Zhang, Z. D., Wang, Y. W., Xu, Q., & Huang, H. (2021b). Recent advances in detoxification strategies for zearalenone contamination in food and feed. *Chinese Journal of Chemical Engineering, 30*, 168–177. https://doi.org/10.1016/j.cjche.2020.11.011

Wang, Y. L., Zhou, X. Q., Jiang, W. W., Wu, P., Liu, Y., Jiang, J., Wang, S. W., Kuang, S. Y., Tang, L., & Feng, L. (2019). Effects of dietary Zearalenone on oxidative stress, cell apoptosis, and tight junction in the intestine of juvenile grass carp (Ctenopharyngodon idella). *Toxins, 11*(6), 333. https://doi.org/10.3390/toxins11060333

Xu, Y., Ma, B., Chen, E. J., Yu, X. P., Ye, Z. H., Sun, C. X., & Zhang, M. Z. (2021). Dual fluorescent immunochromatographic assay for simultaneous quantitative detection of citrinin and zearalenone in corn samples. *Food Chemistry, 336*, 127713. https://doi.org/10.1016/j.foodchem.2020.127713

Yang, R., Li, D. W., Li, A. M., & Yang, H. (2018). Adsorption properties and mechanisms of palygorskite for removal of various ionic dyes from water. *Applied Clay Science, 151*, 20–28. https://doi.org/10.1016/j.clay.2017.10.016

Youcef, L. D., Belaroui, L. S., & López-Galindo, A. (2019). Adsorption of a cationic methylene blue dye on an Algerian palygorskite. *Applied Clay Science, 179*, 105145. https://doi.org/10.1016/j.clay.2017.10.016

Zhang, W., Zhang, S. H., Wang, J. J., Dong, J. W., Cheng, B. J., Xu, L., & Shan, A. S. (2019). A novel adsorbent albite modified with cetylpyridinium chloride for efficient removal of zearalenone. *Toxins, 11*, 674. https://doi.org/10.3390/toxins11110674

Zhang, W., Zhang, L. Y., Jiang, X., Liu, X., Li, Y., & Zhang, Y. G. (2020a). Enhanced adsorption removal of aflatoxin B1, zearalenone and deoxynivalenol from dairy cow rumen fluid by modified nano-montmorillonite and evaluation of its mechanism. *Animal Feed Science and Technology, 259*, 114366. https://doi.org/10.1016/j.anifeedsci.2019.114366

Zhang, Y. Y., Gao, R., Liu, M., Shi, B. M., Shan, A. S., & Cheng, B. J. (2015). Use of modified halloysite nanotubes in the feed reduces the toxic effects of zearalenone on sow reproduction and piglet development. *Theriogenology, 83*(5), 932–941. https://doi.org/10.1016/j.theriogenology.2014.11.027

Zhang, Y., He, J., Song, L., Wang, H., Huang, Z., Sun, Q., & Zhang, S. (2020b). Application of surface-imprinted polymers supported by hydroxyapatite in the extraction of zearalenone in various cereals. *Analytical and Bioanalytical Chemistry, 412*(17), 4045–4055. https://doi.org/10.1007/s00216-020-02610-y

Zhong, H. Q., Mu, B., Zhang, M. M., Hui, A. P., Kang, Y. R., & Wang, A. Q. (2020). Preparation of effective carvacrol/attapulgite hybrid antibacterial materials by mechanical milling. *Journal of Porous Materials, 27*(3), 843–853. https://doi.org/10.1007/s10934-020-00863-7

Zhuang, G. Z., Zhang, Z. P., Jaber, M., Gao, J. H., & Peng, S. M. (2017). Comparative study on the structures and properties of organo-montmorillonite and organo-palygorskite in oil-based drilling fluids. *Journal of Industrial and Engineering Chemistry, 56*, 248–257. https://doi.org/10.1016/j.jiec.2017.07.017

Zuo, R., Meng, L., Guan, X., Wang, J. S., Yang, J., & Lin, Y. H. (2019). Removal of strontium from aqueous solutions by acrylamide-modified attapulgite. *Journal of Radioanalytical and Nuclear Chemistry, 319*(3), 1207–1217. https://doi.org/10.1007/s10967-019-06414-y